

HESS J1640–465 AND HESS J1641–463: TWO INTRIGUING TEV SOURCES IN THE LIGHT OF NEW *FERMI* LAT OBSERVATIONS

M. LEMOINE-GOUMARD^{1,2}, M.-H. GRONDIN^{1,3}, F. ACERO⁴, J. BALLE⁴, H. LAFFON¹, T. REPOSEUR¹

Not to appear in Nonlearned J., 45.

ABSTRACT

We report on γ -ray analysis of the region containing the bright TeV source HESS J1640–465 and the close-by TeV source HESS J1641–463 using 64 months of observations with the *Fermi* Large Area Telescope (LAT). Previously only one GeV source was reported in this region and was associated with HESS J1640–465. With an increased dataset and the improved sensitivity afforded by the reprocessed data (P7REP) of the LAT, we now report the detection, morphological study and spectral analysis of two distinct sources above 100 MeV. The softest emission in this region comes from the TeV source HESS J1641–463 which is well fitted with a power law of index $\Gamma = 2.47 \pm 0.05 \pm 0.06$ and presents no significant γ -ray signal above 10 GeV, which contrasts with its hard spectrum at TeV energies. The *Fermi*-LAT spectrum of the second TeV source, HESS J1640–465 is well described by a power-law shape of index $\Gamma = 1.99 \pm 0.04 \pm 0.07$ that links up naturally with the spectral data points obtained by the High Energy Stereoscopic System (H.E.S.S.). These new results provide new constraints concerning the identification of these two puzzling γ -ray sources.

Subject headings: HESS J1640–465, HESS J1641–463, supernova remnant, pulsar wind nebula, gamma-ray observations

1. INTRODUCTION

HESS J1640–465 is an extended (2.7 ± 0.5 arcmin) γ -ray source detected by the High Energy Stereoscopic System (H.E.S.S.) during its survey of the Galactic Plane (Aharonian et al. 2006). It is centered within the radio supernova remnant (SNR) G338.3–0.0 (Whiteoak & Green 1996). Using X-ray observations with *XMM-Newton* (Funk et al. 2007) and *Chandra* (Lemiere et al. 2009), one compact and one extended X-ray source were detected close to the center of the remnant and within the VHE emission. The compact source was suggested to be a pulsar, and HESS J1640–465 was first interpreted as the associated pulsar wind nebula (PWN), but no pulsation was detected from these datasets. Based on HI absorption features, Lemiere et al. (2009) derived a distance of (8 – 13) kpc, implying a large size for this potential TeV PWN. Later on, observations by the *Fermi*-Large Area Telescope (LAT) revealed a high-energy γ -ray source coincident with HESS J1640–465 (1FGL J1640.8–4634, Slane et al. 2010) with a steep spectrum of index $\Gamma = 2.3 \pm 0.1$. These multi-wavelength data can be reproduced only in the context of a PWN origin if the electron spectrum contains a distinct low-energy component such as a Maxwellian electron population with a power-law tail. More recently, new H.E.S.S. data showed that the VHE γ -ray emission from HESS J1640–465 significantly overlaps the north-western part of the SNR shell of G338.3–0.0 (Abramowski et al. 2014a). In addition, the TeV spectrum connects smoothly with the *Fermi* spectrum and presents a high-energy cut-off, implying that particles with tens of TeV energies are present in the acceleration region. These new data are better explained in a scenario where protons are being accelerated at the shell of SNR G338.0–0.0 and γ -rays

are being produced via proton-proton interaction. To render the whole story even more complex, a few months after this new H.E.S.S. publication, Gotthelf et al. (2014) reported the discovery of pulsations from the X-ray point source previously detected by Funk et al. (2007) and Lemiere et al. (2009) using the Nuclear Spectroscopic Telescope Array (NuSTAR) X-ray observatory. No pulsation was detected using 5 years of *Fermi*-LAT data. However, this new detection restores interest in the scenario of a PWN detected at GeV and TeV energies. Indeed, with a spin-down luminosity of 4.4×10^{36} erg s^{-1} and a characteristic age of 3350 years, this 206 ms pulsar PSR J1640–4631 presents similar properties with the pulsars powering TeV PWNe (Klepser et al. 2013).

Located only $0^{\circ}25'$ away from HESS J1640–465, HESS J1641–463 remained unnoticed using the standard detection technique used by the H.E.S.S. Collaboration. Its detection became possible only by using an energy threshold of 4 TeV (Abramowski et al. 2014b). This new TeV source presents a hard spectrum ($\Gamma \sim 2$), which explains why the distinction between the two TeV sources became more evident above a few TeVs. It is coincident with the radio SNR G338.5+0.1, located at 11 kpc (Kotthes & Dougherty 2007) and adjacent to SNR G338.3–0.0. In radio, the two remnants are connected in projection by the bright HII region G338.4+0.0. No other known counterpart is found to be compatible with HESS J1641–463 and no *Fermi*-LAT source was reported before.

Here, we carried out a complete analysis of this region with *Fermi*-LAT data accumulated over 5 years using the most recent instrument response functions (IRFs) and diffuse background models. In Section 2, we describe the γ -ray observations used, while Section 3 presents the results obtained from a detailed morphological and spectral analysis of the *Fermi*-LAT data. Finally, in Section 4, we discuss the main implications of these results concerning the origin of the detected γ -ray signal.

2. LAT DESCRIPTION AND OBSERVATIONS

The LAT is an electron-positron pair-conversion telescope, sensitive to γ -rays with energies from 20 MeV to more than

arXiv:1409.4994v1 [astro-ph.HE] 17 Sep 2014

¹ Centre d'Études Nucléaires de Bordeaux Gradignan, IN2P3/CNRS, Université Bordeaux 1, BP120, F-33175 Gradignan Cedex, France

² email: lemoine@cenbg.in2p3.fr

³ email: grondin@cenbg.in2p3.fr

⁴ Laboratoire AIM, CEA-IRFU/CNRS/Université Paris Diderot, Service d'Astrophysique, CEA Saclay, 91191 Gif sur Yvette, France

300 GeV (Atwood et al. 2009).

The following analysis was performed using more than 5 years of *Fermi*-LAT reprocessed Pass 7 data collected primarily in survey mode (2008 August 04 – 2013 December 4). This new dataset consists of Pass 7 LAT data that have been reprocessed using updated calibration constants for the detector systems (Bregeson et al. 2013). Only γ rays in the Source class events were selected, excluding those coming from a zenith angle larger than 100° to the detector axis to reduce contamination from the Earth limb. We adopted the P7REP_SOURCE_V15 IRFs.

3. FERMI-LAT ANALYSIS OF HESS J1640–465 AND HESS J1641–463

The spatial and spectral analysis of the γ -ray data is performed using two different tools, *gtlike* and *pointlike*. *gtlike* is a maximum-likelihood method (Mattox et al. 1996) implemented in the Science Tools distributed by the *Fermi* Science Support Center (FSSC)⁵. *pointlike* is an alternate binned likelihood technique, optimized for characterizing the extension of a source (unlike *gtlike*), that was extensively tested against *gtlike* (Kerr 2011; Lande et al. 2012). These tools fit a model of the region, including sources, residual charged particles, extragalactic and Galactic backgrounds, to the data. For this work, the Galactic diffuse emission model *gll_iem_v05.fits* and isotropic diffuse model *iso_source_v05.txt* provided by the *Fermi*-LAT Collaboration were used⁶. Sources within 20° of HESS J1640–465 are extracted from an internal 4-year source list and used in the likelihood fit. The spectral parameters of sources closer than 5° to HESS J1640–465 (located at the center of our square region of interest of 10° half-side) are left free, while the parameters of all other sources are fixed at the values from the 4-year list.

3.1. Morphological analysis

Two sources are detected in the 4-year list, positionally coincident with HESS J1640–465 and HESS J1641–463. To have a better understanding of this complex region, we first generated residual Test Statistic (TS) maps in three different energy bands using *pointlike*: 0.3 – 3 GeV, 3 – 30 GeV, 30 – 300 GeV. The low energy threshold of 0.3 GeV was defined as a good compromise between statistics and angular resolution. $TS = 2(\log \mathcal{L}_1 - \log \mathcal{L}_0)$ where \mathcal{L}_1 is the likelihood obtained by fitting the source plus background model to the data, and \mathcal{L}_0 is obtained by fitting the background alone (Mattox et al. 1996). For each energy band, this skymap contains the TS value for a point source at each map location assuming a fixed photon index $\Gamma = 2$, thus giving a measure of the statistical significance for the detection of a γ -ray source in excess of the background. The diffuse Galactic and isotropic emission, as well as nearby sources (except the two sources coincident with our two TeV sources of interest) are included in the background model. The resulting RGB composite TS map (Figure 1) clearly shows a γ -ray signal coincident with the position of HESS J1641–463 in the 3 – 30 GeV energy range, while the only remaining γ -ray emission in the 30 – 300 GeV energy band is coincident with HESS J1640–465. This is a very good indication that, indeed, two components are visible with *Fermi*-LAT and that the γ -ray emission coming from HESS J1640–465 may be harder.

⁵ <http://fermi.gsfc.nasa.gov/ssc/>

⁶ These models are available at : <http://fermi.gsfc.nasa.gov/ssc/data/access/lat/BackgroundModels.html>

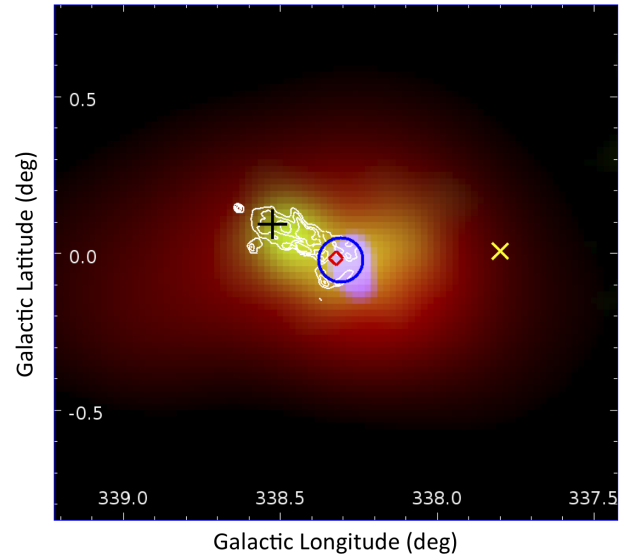


FIG. 1.— *Fermi*-LAT composite TS map of the region containing the two TeV sources in the 0.3 – 3.0 (red), 3.0 – 30.0 GeV (green) and 30.0 – 300.0 GeV (blue) energy ranges, in Galactic coordinates. The best position of the H.E.S.S. point source HESS J1641–463 is marked with a black plus while the best position and extension of the H.E.S.S. Gaussian HESS J1640–465 is represented by a blue circle. The red diamond indicates the position of the pulsar PSR J1640–4631, while the yellow cross shows the position of the only close-by source from the internal *Fermi*-LAT source list located in the region. Radio continuum at 843 MHz is shown as white contours (Whiteoak & Green 1996). The maximal TS values are 255, 100, 43 for the red, green and blue maps respectively.

In a second step, to ensure that the two sources are significantly detected and check their possible extension, we used *pointlike* above 3 GeV, thus only keeping events with the best angular reconstruction. We tested different hypotheses to represent the emission coming from HESS J1640–465 and HESS J1641–463: one point source (model *A*), one Gaussian distribution (model *B*), one Gaussian distribution with two power-law type components (model *C*), two point sources (model *D*), and one Gaussian plus one point source (model *E*). We also used the best spatial shape (1-D Gaussian) representing HESS J1640–465 as observed by H.E.S.S. (model *F*, Abramowski et al. 2014a), and another spatial model composed of this best Gaussian distribution and the best-fit position of a point source for HESS J1641–463 (model *G*, also obtained by H.E.S.S., Abramowski et al. 2014b). For all these tests, power-law spectral shapes were assumed. The results of the extension fits and the improvement of the TS when using spatially extended models are summarized in Table 1, along with the number of additional degrees of freedom with respect to the null hypothesis. The 5σ improvement of the likelihood fit between a Gaussian distribution and the Gaussian plus point-source hypothesis (difference in TS of 36 for 4 additional degrees of freedom) supports the conclusion that two different components are detected in this region and, above all, that a significant γ -ray source is located in the vicinity of HESS J1641–463. This is the first time that a detection of this source is reported at these energies. The improvement when using a Gaussian plus a point source instead of the two point-source hypothesis is marginal (2.4σ) and therefore one cannot exclude the possibility that both sources are point-like in the GeV energy range. However, in both hypotheses (*D* and *E*), the best-fit positions obtained with the *Fermi*-LAT data are in good agreement with those extracted from

TABLE 1
CENTROID AND EXTENSION FITS OF THE LAT DATA USING `pointlike` ABOVE 3 GeV.

	Spatial Model	R.A. (°)	Dec. (°)	σ (°)	TS (3 – 300 GeV)	N.d.o.f.**
<i>A</i>	1 Point Source	250.14	–46.56		148	4
<i>B</i>	1 Gaussian Source	250.17	–46.52	0.12	186	5
<i>C</i>	1 Gaussian Source with 2 power-law type components	250.17	–46.52	0.12	191	7
<i>D</i>	2 Point Sources	250.13 / 250.27	–46.57 / –46.35		216	8
<i>E</i>	1 Gaussian + 1 Point Source	250.15 / 250.27	–46.59 / –46.34	0.06 / –	222	9
<i>F</i>	HESS J1640–465 Gaussian*	250.17	–46.54	0.07	166	2
<i>G</i>	HESS J1640–465 Gaussian* + HESS J1641–463 Point Source*	250.17 / 250.26	–46.54 / –46.30	0.07 / –	208	4

* H.E.S.S. positions and extensions are fixed to the values from Abramowski et al. (2014a) and Abramowski et al. (2014b).

** N. d.o.f. : number of degrees of freedom.

H.E.S.S. analyses (Abramowski et al. 2014a,b). In model *E*, the best-fit position for the Gaussian is $\alpha(\text{J2000}) = 250^\circ.15$, $\delta(\text{J2000}) = -46^\circ.59$ with a 68% error radius of $0^\circ.02$, and an extension of $0^\circ.06 \pm 0^\circ.02$. The best-fit position for the additional point source is $\alpha(\text{J2000}) = 250^\circ.27$, $\delta(\text{J2000}) = -46^\circ.34$ with a 68% error radius of $0^\circ.02$. Since this model (*E*) is not significantly better than the same model with parameters fixed to the values extracted from Abramowski et al. (2014a) and Abramowski et al. (2014b), at the expense of a larger number of degrees of freedom, we decided to use the H.E.S.S. spatial shapes (model *G*) to derive the spectra of both sources.

3.2. Spectral analysis

The following spectral analysis was performed with `gtlike` using all events between 0.1 and 300 GeV. As discussed in Section 3.1, we used the spatial model *G* from Table 1 to represent the γ -ray emission observed by the LAT from HESS J1640–465 and HESS J1641–463. Assuming this spatial shape, the γ -ray sources observed by the LAT above 100 MeV are detected with a TS of 148 for HESS J1640–465 and 105 for HESS J1641–463. Their spectra are presented in Figures 2 and 3. They are both well described by simple power laws ($dN/dE \propto E^{-\Gamma}$) with spectral indices of $\Gamma = 1.99 \pm 0.04 \pm 0.07$ for the source HESS J1640–465 and $\Gamma = 2.47 \pm 0.05 \pm 0.06$ for the source HESS J1641–463. This confirms the trend of a harder spectrum for HESS J1640–465, as suggested by Figure 1 and further discussed in Section 3.1. The integrated flux above 100 MeV is $(4.5 \pm 0.2 \pm 0.2) \times 10^{-5} \text{ MeV cm}^{-2} \text{ s}^{-1}$ for HESS J1640–465 and $(2.6 \pm 0.2 \pm 0.5) \times 10^{-5} \text{ MeV cm}^{-2} \text{ s}^{-1}$ for HESS J1641–463. The first error is statistical, while the second represents our estimate of systematic effects as discussed below. No evidence of variability was found for these two sources by dividing the data into yearly time bins and applying the likelihood procedure for each.

The *Fermi*-LAT spectral points shown in Figures 2 and 3 were obtained by dividing the 0.1 – 300 GeV range into 14 logarithmically spaced energy bins and performing a maximum likelihood spectral analysis in each interval, assuming a power-law shape with fixed photon index $\Gamma = 2$ for both sources. The normalizations of the diffuse Galactic and isotropic emission were left free in each energy bin as well as those of sources located within 5° from HESS J1640–465. A 95% C.L. upper limit is computed when the statistical significance is lower than 2σ . At the highest energies, bins corresponding to upper limits were combined. The errors on the spectral points represent the statistical and systematic uncertainties added in quadrature.

Two main systematic errors have been taken into account: imperfect modeling of the Galactic diffuse emission and uncertainties in the effective area calibration. The first was estimated by comparing the results obtained using the standard Galactic diffuse model with the results based on eight alternative interstellar emission models as performed in de Palma et al. (2013). The second is estimated by using modified IRFs whose effective areas bracket the nominal ones. These bracketing IRFs are defined by envelopes above and below the nominal energy dependence of the effective area by linearly connecting differences of (10%, 5%, 5%, 15%) at $\log_{10}(E/\text{MeV})$ of (2, 2.5, 4, 6), respectively⁷.

4. DISCUSSION

Thanks to a larger dataset and to an improved event reconstruction, *Fermi*-LAT analysis of the region containing the two TeV sources HESS J1640–465 and HESS J1641–463 has led to the detection of two distinct GeV sources of γ -ray photons. The first one, coincident with HESS J1640–465 presents a hard spectrum, while the second one shows a much steeper spectrum. These new characteristics can be used to constrain the natures of these two γ -ray sources. In the following, we will assume that HESS J1640–465 is located at 10 kpc (as in Abramowski et al. 2014a) and that HESS J1641–463 is 11 kpc from us (following Abramowski et al. 2014b).

For the case of HESS J1640–465, the hard spectrum revealed in this new analysis connects perfectly with the TeV spectral points (see Figure 2). The resulting γ -ray luminosity above 100 MeV for this source is $L_{\geq 100 \text{ MeV}} \approx (6.8 \pm 0.6) \times 10^{35} (D/10 \text{ kpc})^2 \text{ erg s}^{-1}$; this is three times less than reported by Slane et al. (2010). This significant change is mainly due to the large contamination below 1 GeV implied by the close-by source HESS J1641–463, which shows a much steeper spectrum in this energy band. The high γ -ray luminosity and flat spectral shape of HESS J1640–465 is typical of SNRs interacting with molecular clouds previously detected with *Fermi*, such as IC 443 and W51C, which both have luminosities $\geq 10^{35} \text{ erg s}^{-1}$ (Abdo et al. 2010, 2009b). The new *Fermi*-LAT data thus strengthen the SNR scenario discussed in Abramowski et al. (2014a) where protons are accelerated in the shell of SNR G338.3–0.0 and the γ -ray emission from HESS J1640–465 arises from the interaction region between the blast wave and the G338.4+0.1 H II complex. In the framework of such hadronic scenario, we calculated the flux and spectrum of the γ rays produced by π^0 -decay following the analytical approximations by Kelner et al. (2006), as

⁷ http://fermi.gsfc.nasa.gov/ssc/data/analysis/LAT_caveats.html

suming a gas density of 150 cm^{-3} (Abramowski et al. 2014a). The particle index is fixed at 2.0 (in agreement with the spectral index derived in this work) with an energy cut-off at 50 TeV taking into account the spectral curvature observed by H.E.S.S. at TeV energies. The total energy in cosmic-ray (CR) hadrons required to reproduce the *Fermi*-LAT and H.E.S.S. data (see dashed line in Figure 2) is $\frac{0.8}{f} \times 10^{50}$ erg, where f corresponds to the fraction of the SNR that is interacting with the molecular cloud. In case of full immersion ($f = 1$) and for a typical explosion energy of $\sim 10^{51}$ erg, this hadronic model indicates that only $\sim 8\%$ of the initial kinetic energy needs to be transferred to CRs. Since f is a poorly known fraction, the derived energy should be considered as a lower limit. The high density needed and the high-energy cut-off visible in this source contrast with other *Fermi*-LAT detected SNRs.

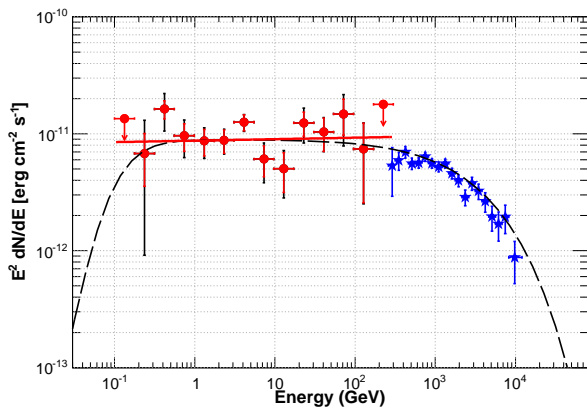


FIG. 2.— Gamma-ray spectra of HESS J1640–465, using the best Gaussian spatial model from Abramowski et al. (2014a). The red line shows the fit of a power-law to the *Fermi* spectrum derived above 100 MeV. The red data points (crosses) indicate the fluxes measured in each of the 14 energy bins indicated by the extent of their horizontal lines. The statistical errors are shown in red, while the black lines take into account both the statistical and systematic errors as discussed in Section 3.2. A 95% C.L. upper limit is computed when the statistical significance is lower than 2σ . The blue data points are taken from Abramowski et al. (2014a). The dashed black line indicates the hadronic model discussed in Section 4.

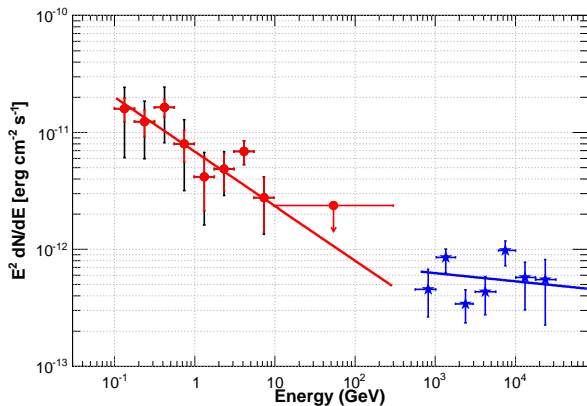


FIG. 3.— Gamma-ray spectra of HESS J1641–463, using the best point source position from Abramowski et al. (2014b). Same conventions as for Figure 2. The blue data points and the best spectral fit (represented as a blue line) are taken from Abramowski et al. (2014b).

One cannot exclude the possibility that part of the flux detected by *Fermi* is produced by PSR J1640–4631 or even by its PWN in SNR G338.3–0.0, which would further decrease these values. In the case of contamination by PSR J1640–4631, though no pulsation was detected by Gotthelf et al. (2014) in the *Fermi*-LAT data, the absence of spectral curvature or cut-off up to 300 GeV in the *Fermi* source implies that the bulk of the emission does not arise from this pulsar, especially above 10 GeV. The PWN scenario is more likely, and it is interesting to note that the PWN modeling presented in Gotthelf et al. (2014) reproduces relatively well the high-energy end of the spectrum obtained in our new analysis (above a few GeV). In this context, the marginally significant extension indicated by our analysis would be an important argument in favor of the PWN or the SNR scenario, if it is confirmed with more data.

In the case of HESS J1641–463, the connection between the steep spectrum detected by this new analysis and the H.E.S.S. spectrum remains unclear and points toward two different mechanisms or sources producing the γ -ray photons detected in each energy band. This recalls the case of HESS J1356–645, within which *Fermi*-LAT detects the pulsed emission of PSR J1357–6429 while, at TeV energies, H.E.S.S. observes its associated PWN (Abramowski et al. 2011). In such a PSR/PWN scenario, the flux density of the X-ray source nearest to HESS J1641–463 is a factor 15 less energetic when compared with the energy flux density of the TeV source (Abramowski et al. 2014b), which would resemble the numerous associations of dark TeV sources and weak X-ray synchrotron PWN that have been established so far. Another possibility in such a “two source” scenario, emphasized by the good positional coincidence between HESS J1641–643 with SNR G338.5+0.1, would be that the γ -ray photons detected at TeV energies are produced by accelerated protons from this SNR interacting with the ambient gas, as suggested by Abramowski et al. (2014b), while *Fermi* would be seeing a contaminating pulsar. Finally, another scenario would be that HESS J1641–463 is a binary system similar to LS 5039 and LSI +61°303, both showing a pulsar-like spectrum at GeV energies that does not connect to the TeV spectrum (Hadasch et al. 2012). In this regard, the non detection of spectral curvature and/or variability with the current *Fermi*-LAT dataset does not permit excluding this last scenario since the GeV source is rather weak and the statistics are too low to perform a blind search for pulsation or to divide the dataset into intervals shorter than one year.

Further observations as well as timing and flux variability searches with *Fermi* and H.E.S.S. and also with high-resolution X-ray instruments will be key to finally understanding the nature of these two intriguing γ -ray sources.

The *Fermi* LAT Collaboration acknowledges generous ongoing support from a number of agencies and institutes that have supported both the development and the operation of the LAT as well as scientific data analysis. These include the National Aeronautics and Space Administration and the Department of Energy in the United States, the Commissariat à l’Energie Atomique and the Centre National de la Recherche Scientifique / Institut National de Physique Nucléaire et de Physique des Particules in France, the Agenzia Spaziale Italiana and the Istituto Nazionale di Fisica Nucleare in Italy, the Ministry of Education, Culture, Sports, Science and Technology (MEXT), High Energy Accelerator Research Organiza-

tion (KEK) and Japan Aerospace Exploration Agency (JAXA) in Japan, and the K. A. Wallenberg Foundation, the Swedish Research Council and the Swedish National Space Board in Sweden.

Additional support for science analysis during the opera-

tions phase from the following agencies is also gratefully acknowledged: the Istituto Nazionale di Astrofisica in Italy and the Centre National d'Études Spatiales in France.

REFERENCES

- Abdo, A. A., Ackermann, M., Ajello, M. et al. 2010, *ApJ*, 712, 459
 Abdo, A. A., Ackermann, M., Atwood, W. B., et al. 2009a, *Astroparticle Physics*, 32, 193
 Abdo, A. A., Ackermann, M., Ajello, M. et al. 2009b, *ApJL*, 706, L1
 Abramowski, A., Acero, F., Aharonian, F. et al. (H.E.S.S. Collaboration), 2011, *A&A*, 533, 103
 Abramowski, A., Aharonian, F., Ait Benkhali, F. et al. (H.E.S.S. Collaboration), 2014a, *MNRAS*, 439, 2828
 Abramowski, A., Aharonian, F., Ait Benkhali, F. et al. (H.E.S.S. Collaboration), 2014b, arXiv:1408.5280
 Aharonian F., Akhperjanian, A. G., Bazer-Bachi, A. R. et al. (H.E.S.S. Collaboration), 2006, *ApJ*, 636, 777
 Atwood, W. B., Abdo, A. A., Ackermann, M., et al. 2009, *ApJ*, 697, 1071
 Bregeon, J., Charles, E., & M. Wood for the Fermi-LAT collaboration, 2013, proceedings of the Fermi Symposium, arXiv:1304.5456
 Funk S., Hinton J. A., Pühlhofer G., Aharonian F. A., Hofmann W., Reimer O., Wagner S., 2007, *ApJ*, 662, 517
 Gotthelf, E. V., Tomsick, J. A., Halpern, J. P., et al., 2014, *ApJ*, 788, 155
 Hadasch, D., Torres, D. F., Tanaka, T. et al. 2012, *ApJ*, 749, 54
 Kelner, S. R., Aharonian, F. A., & Bugayov, V. V., 2006, *Phys. Rev. D*, 74, 034018
 Kerr, M. 2011, PhD Thesis, arXiv:1101.6072v
 Klepser, S. et al., 2013, proceedings of the 33rd International Cosmic Ray Conference, arXiv:1307.7905
 Kothes, R. & Dougherty, S. M. 2007, *A&A*, 468, 993
 Lande, J., Ackermann, M., Allafort, A. et al., 2012, *ApJ*, 756, 5
 Lemièrè A., Slane P., Gaensler B. M., Murray S., 2009, *ApJ*, 706, 1269
 Mattox, J. R., Bertsch, D. L., Chiang, J. et al., 1996, *ApJ*, 461, 396
 de Palma, F., Brandt, T. J., Johannesson, G., Tibaldo, L. for the Fermi LAT collaboration 2013, arXiv:1304.1395
 Slane P., Castro D., Funk S., Uchiyama Y., Lemièrè A., Gelfand J. D., Lemoine-Goumard M., 2010, *ApJ*, 720, 266
 Smith D. A., Guillemot, L., Camilo, F. et al. 2008, *A&A*, 492, 3
 Whiteoak J. B. Z. & Green A. J., 1996, *A&AS*, 118, 329